

See discussions, stats, and author profiles for this publication at: <https://www.researchgate.net/publication/231647978>

Electrical Characteristics of Cobalt Phthalocyanine Complexes Adsorbed on Graphene

ARTICLE in THE JOURNAL OF PHYSICAL CHEMISTRY C · JULY 2011

Impact Factor: 4.77 · DOI: 10.1021/jp2041026

CITATIONS

18

READS

87

4 AUTHORS, INCLUDING:



Gloria Cardenas-Jiron

University of Santiago de Chile (USACH), San...
Chile

68 PUBLICATIONS 964 CITATIONS

[SEE PROFILE](#)



Diego Cortés-Arriagada

Pontifical Catholic University of Chile
Chile

15 PUBLICATIONS 56 CITATIONS

[SEE PROFILE](#)



Jorge Seminario

Texas A&M University
USA

232 PUBLICATIONS 4,962 CITATIONS

[SEE PROFILE](#)

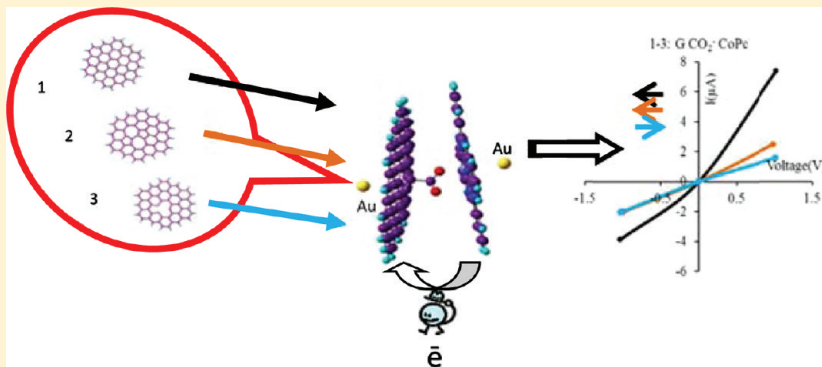
Electrical Characteristics of Cobalt Phthalocyanine Complexes Adsorbed on Graphene

Gloria I. Cárdenas-Jirón,^{†,||} Paola Leon-Plata,[†] Diego Cortes-Arriagada,^{||} and Jorge M. Seminario^{*,†,‡,§}

[†]Department of Chemical Engineering, [‡]Department of Electrical and Computer Engineering, and [§]Materials Science and Engineering Program, Texas A&M University College Station, Texas, USA

^{||}Laboratorio de Química Teórica, Departamento de Ciencias del Ambiente, Facultad de Química y Biología, Universidad de Santiago de Chile (USACH), Casilla 40, Correo 33, Santiago, Chile

ABSTRACT:



We investigate, at a density functional level, the electric characteristics of 18 complexes of cobalt phthalocyanine (CoPc) and cobalt tetraaminephthalocyanine (CoTAPc) adsorbed on graphene functionalized with CO_2^- or CO moieties. Three models of graphene molecules are used, pristine, defect, and vacancy, leading to 12 complexes with CO_2^- functionalized graphene and 6 complexes with functionalized CO graphene. The molecular structures of the optimized complexes feature covalent adsorption Co–O lengths of $\sim 1.9\text{--}2.1\text{ \AA}$ and C–N lengths of $\sim 1.4\text{ \AA}$ in parallel, perpendicular, and coplanar structures of graphene with phthalocyanine. All these conformations have a direct effect on the electronic characteristics of the complexes. Binding energies calculated for the interaction between functionalized graphene and phthalocyanine show that structures with defects and vacancies have lower energies than pristine graphene. In particular, we found that complexes having a graphene-CO linked to phthalocyanine by an amide bond are of highest stability (by $\sim 130\text{ kcal/mol}$) and the formation of complexes with CO_2^- functionalized graphenes takes place preferably when involved with CoTAPc (by $\sim 20\text{ kcal/mol}$). Frontier molecular orbitals (HOMO and LUMO) suggest that several of these complexes behave as charge transfer compounds with phthalocyanine as an electron donor and graphene as an electron acceptor, thus these complexes could behave as sensors because of the absorption properties of phthalocyanine in the UV–vis region. The calculated current–voltage characteristics show that electron transfer is preferably favored in complexes with parallel structure and with pristine graphene CO_2^- functionalization ($\sim 7\text{ }\mu\text{A}$) when both conjugates, graphene and phthalocyanine, face each other. The latter implies the transfer of charge through a $\pi-\pi$ setting. However, the presence of defects and vacancies, for this face to face structure, shows lower electron transfer, having G-Def and G-Vac similar values of electron transfer. The conduction is very low for complexes with high stability (usually the coplanar structures) and with charge transfer features, i.e., those in which the HOMO and LUMO are in separated parts of the complex (usually the perpendicular and the coplanar structures). This study shows that cobalt phthalocyanine conducts electrical current toward graphene through a covalently attached CO_2^- to the graphene.

1. INTRODUCTION

Pristine graphene (G) is a flat two-dimensional structure¹ of carbon atoms with unique mechanical and electronic properties due to its rigid hexagonal sp^2 rings, allowing a conjugation through their π molecular orbitals, which yield excellent conduction properties, even superior to those of carbon nanotubes.^{2–6}

Individual graphene sheets have been characterized by transmission electron microscopy, which revealed that these sheets are not perfectly flat; on the contrary, they show intrinsic microscopic roughening with out-of-plane deformations in the order of

1 nm^7 and can be used in any of the scenarios for molecular electronics.⁸

Graphene surfaces may feature alterations, defects (Def), or vacancies (Vac) that affect their electronic properties as it has been showed for a monovacancy, a divacancy, and a Stone–Wales defects using calculated Raman spectra density functional theory

Received: May 3, 2011

Revised: July 6, 2011

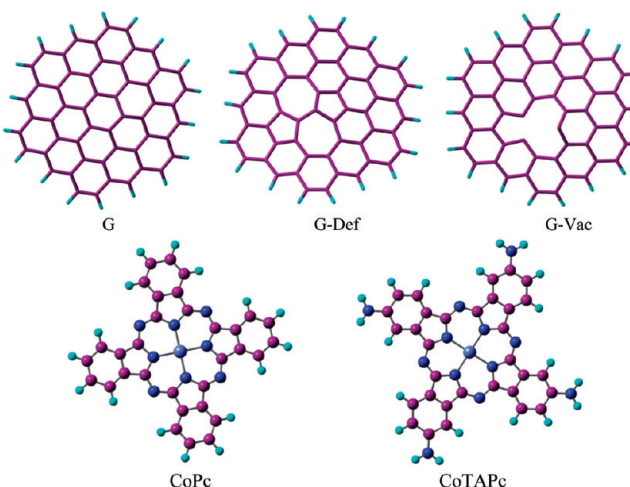


Figure 1. Graphene structural models (G, Def, and Vac) and cobalt phthalocyanines (CoPc and CoTAPc). Color code showed in Figure 2.

(DFT) with a nonorthogonal tight-binding model;⁹ it was found that the Raman intensity can be enhanced up to 1 order of magnitude by the presence of defects in comparison with a pristine graphene,⁹ and these spectra can serve as signatures for specific defects.

It has been shown that Stone–Wales (SW) defects yield changes in the electronic properties of graphene and affect the reactivity toward the adsorption of adsorbates.^{3,5,7,9–29} It is also known that the presence of vacancies in graphene nanoribbons modifies the electronic transport properties, affecting the conductance of these nanomaterials.^{2,14,30–35} A study on multi-vacancies in carbon nanotubes has also revealed the existence of stability at magic numbers.³³ Graphene-based complexes have been explored in energy conversion,³⁶ electrical conduction,¹⁴ solubility,³⁷ and composites formation.^{31,38–40}

Carboxylic acid-functionalized graphene nanosheets have been obtained by chemical reduction of graphite oxide and used to build together amine-functionalized graphene nanosheet thin films of graphene via layer-by-layer assembly through electrostatic interactions, which can have applications such as transparent electrodes and highly sensitive biosensors.⁴¹ Other studies report carboxylic-acid-functionalized graphene as biosensors for simultaneous determination of adenine and guanine in DNA.³⁹

The mechanism of chemical functionalization of pristine, vacancy, and SW defect graphene models through COOH groups has also been studied using density functional theory,⁴² whereby the attachment of functional groups is stronger in graphene with SW defects and vacancies as justified by its larger binding energy than pristine graphene. Chemical functionalization of graphene oxide with porphyrin TPP-NH₂ (5-(aminophenyl)-10,15,20-triphenylporphyrin) has been reported and confirmed using FTIR, UV-vis absorption, and TEM studies, indicating that these molecules are covalently connected through one amide bond.^{19,37} Thus, multifunctional materials at nanometer-scale can take advantage of porphyrin as it improves the solubility of graphene in organic solvents in addition to its optoelectronic and catalytic properties.

Some works have been reported for the adsorption of phthalocyanines on graphene; reduced graphene oxide (RGO) composites containing tetrasulfonate salt of copper phthalocyanine (TSCuPc), which have been fabricated and could be used as

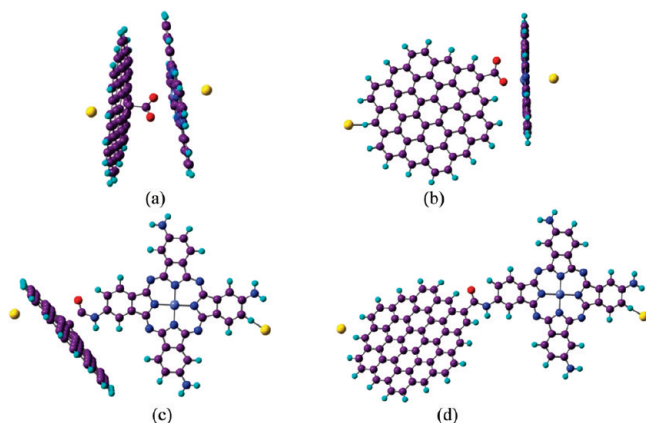


Figure 2. G and CoPc (CoTAPc) complexes attached to Au atoms. (a) **1'**, G-CO₂⁻-CoPc-Au₂; (b) **7'**, G-CO₂⁻-LAT-CoPc-Au₂; (c) **13'**, G-CO-CoTAPc-Au₂; and (d) **16'**, G-CO-LAT-CoTAPc-Au₂. Color code: carbon (purple), hydrogen (cyan), nitrogen (blue), oxygen (red), cobalt (steel blue), and gold (yellow).

optoelectronics devices. These composites have higher photoconductivity and photoresponsivity than RGO films because the presence of donor/acceptor materials and large donor/acceptor (D/A) interfaces for charge generation.¹⁷ Iron phthalocyanine molecules have been observed by scanning tunneling microscopy (STM) to be self-assembled on a monolayer graphene, demonstrating that the latter can act as a template for the fabrication of unique nanoarchitectures with interesting properties.³⁸

In this work, we investigate the adsorption of cobalt phthalocyanine (CoPc) and cobalt tetraaminephthalocyanine (CoTAPc) on functionalized graphene with carboxylate anion (CO₂⁻) or carbonyl group (CO). We used several models of graphene (Figure 1) and studied how the electrical properties of the complexes G-CO₂⁻(CO)-CoPc(CoTAPc) are modulated by the defects in graphene.

2. METHODOLOGY

Using three structural models of graphene, G, G-Def, and G-Vac functionalized with CO₂⁻ or CO and two phthalocyanines (Figure 1), we built 18 complexes. The attachments between graphene and metal phthalocyanine are classified as cobalt-centered and ligand centered, whether the link to graphene occurs through the cobalt atom (complexes **1–12**), or rather through the boundary of phthalocyanine ligand (complexes **13–18**). As graphene models (Figure 1), we consider a pristine graphene (G) with 19 hexagonal rings, a cluster containing Stone–Wales (SW) defects (G-Def),⁴³ where four hexagons become two heptagons and two pentagons, and a cluster of graphene with vacancy (G-Vac), containing 16 hexagons and one dodecagon.

Figure 2 shows the four conformations of the complex structures of graphene and phthalocyanine: two cobalt-centered (a) parallel and (b) perpendicular, and two ligand-centered (c) perpendicular and (d) coplanar. These complexes are augmented with two gold atoms (the numerical bolded label of molecules extended with gold atoms appears primed) used as interface to electrodes, in which a voltage difference is applied to the complexes. Thus, complex **1'** shows graphene functionalized with CO₂⁻ at its center, and cobalt phthalocyanine in parallel conformation and linked through the cobalt. However, in **7'** the

conformation of graphene with cobalt phthalocyanine is nearly perpendicular and CO_2^- graphene functionalization is at the edge of the graphene. For complexes **13'** and **16'** the graphene is functionalized with CO at the center and edge of graphene, respectively, and it is linked to phthalocyanine through the amine group localized at phthalocyanine ligand boundary; thus, the phthalocyanine in **13'** is perpendicular and in **16'** both conjugates have coplanar conformations.

All complexes are optimized in two stages; first we do an optimization of all graphene models functionalized (with CO_2^- and CO), and then these structures are used to build up the complexes. The relaxation of all complexes is carried out considering the optimized graphene model frozen; in the case of **1–6** the carbon atom attached to graphene is also frozen to prevent CO_2^- goes away.

For the binding energy calculation of graphene with phthalocyanine, we carried out the optimization of the complexes isolated fragments (functionalized graphenes and phthalocyanines). Cobalt atom is in oxidation state II in both structures, CoPc and CoTAPc, and then the spin multiplicity used for these compounds is 2. Complexes **1–12** are calculated with a total charge (Q) of -1 ; **1–6** as singlets and **7–12** as doublets. For **13–18**, we use $Q = 0$ and with **13–15** as singlets and **16–18** as doublets.

The optimization on each complex and fragment is performed with the program Gaussian 03²³ using density functional theory with the B3LYP exchange correlation functional^{44–47} and the 6-31G⁴⁸ basis set for C, N, H, and O; the quasi-relativistic pseudopotential and basis set LANL2DZ^{49–51} is used for cobalt.

We model an electric circuit placing two gold atoms at each side of the conjugated structures (augmented complexes) connecting them to nanosized electrodes. Gold contacts are placed at the same distance and in the proximity of the same atom for complexes of the same conformation as shown in Figure 2. In all cases the electrodes are exactly of the same nature in order to have a consistent comparison among all complexes.

DFT calculations are carried out to the augmented complexes including an external electric dipole fields that yields a bias voltage (V) between the gold contacts using the program Gaussian 09.¹⁵ For the external voltage biased structures, we use the hybrid functional B3PW91, which uses a combination of Becke3 (B3)⁴⁴ exchange functional Hartree–Fock (HF) exchange and Perdew–Wang (PW91)^{52–56} correlation functional. The quasi-relativistic pseudopotential and basis sets LANL2DZ^{49–51} is used for Au and Co atoms, and the 6-31G(d)^{57,58} basis set for C, N, O, and H atoms. The use of the LANL2DZ has been successfully used in the past for other transition metals.^{59–63} Most of the methods used in this work have been widely tested, for instance with energetic materials,^{64–70} with transition metals,^{60–63} and with molecular electronics,^{71–74} among others.

The density of states (DOS) of the bulk contacts is calculated with the program Crystal-06,^{75,76} which uses DFT with periodic boundary conditions. The continuum DOS is combined with the Hamiltonian and overlap matrices of the augmented complexes calculated with the Gaussian 09¹⁵ at each bias voltage. The Green's function procedure encoded in the program GENIP⁷⁷ is used to calculate the current–voltage characteristics of the complexes, in addition to the DOS and transfer functions of the junctions (complexes plus electrodes). GENIP uses the discrete (augmented molecule) and the continuous (bulk contacts) in a Green's function technique to determine the electron transport through single molecules^{22,34,35,78,79} and several nanojunctions;^{30,34,35,80} for details see refs 26, 78, and 81 and

references therein; the procedure is summarized as follows, The Green's function for the problem can be obtained from

$$H_{\text{KS}}(V)\psi(V) = E(V)S(V)\psi(V) \quad (1)$$

where the Hamiltonian $H_{\text{KS}}(V)$ and overlap matrices $S(V)$ are calculated at each applied voltage V . The Hamiltonian can be partitioned into the electrodes (1 and 2) and the molecule (M)

$$H_{\text{KS}}(V) = \begin{bmatrix} H_{11}(V) & H_{1\text{M}}(V) & H_{12}(V) \\ H_{\text{M}1}(V) & H_{\text{MM}}(V) & H_{\text{M}2}(V) \\ H_{21}(V) & H_{2\text{M}}(V) & H_{22}(V) \end{bmatrix} \quad (2)$$

where H_{ij} (for $i \neq j$) refer to submatrices representing the coupling between electrodes and the molecule. In particular, we assume that the two electrodes do not interact with each other, thus $H_{12} = H_{21} = 0$.

Thus, the Green's function for the junction becomes

$$G(E, V) = 1/[E(V)S(V) - H_{\text{KS}}(V)]$$

The Green's function for the standalone molecule, G_M , is obtained from the full Green function $G(E, V)$ of the molecular junction,⁷⁷ using the H and S matrices taken from the augmented molecule, as a function of the energy E of the crossing electron at each applied voltage

$$G(E, V) = \begin{bmatrix} g_1^{-1} & -\tau_1 & 0 \\ -\tau_1^+ & ES_{\text{MM}}(V) - H_{\text{MM}}(V) & -\tau_2^+ \\ 0 & -\tau_2 & g_2^{-1} \end{bmatrix} = \begin{bmatrix} G_1 & G_{1\text{M}} & G_{12} \\ G_{\text{M}1} & G_M & G_{2\text{M}} \\ G_{21} & G_{\text{M}2} & G_2 \end{bmatrix} \quad (3)$$

where $\tau_i = (ES_{i\text{M}} - H_{i\text{M}})$, S_{MM} is the overlap submatrix and H_{MM} is the Hamiltonian of the standalone molecule. The complex green function g_i for the contact i , is defined as

$$gt(E) = -\pi\sqrt{-1} \begin{bmatrix} g_i^1 & \dots & 0 \\ \vdots & \ddots & \vdots \\ 0 & \dots & g_i^{n_i} \end{bmatrix} \quad (4)$$

where the g_i^k are diagonal matrices of DOS for each atom k of the n_i gold atoms at each electrode i (in our calculations, we used one gold atom at each electrode); thus, each g_i^k corresponds to the contributions from the s, p, d_{z^2} , and d_{eg} characters of the electrodes DOS's, which is calculated using DFT to solve the Schrodinger equation under periodic boundary conditions with the program Crystal-06.^{75,76}

From eq 3, we get

$$G_M(E, V) = [ES_{\text{MM}}(E, V) - H_{\text{MM}}(E, V) - \sum_1(E, V) - \sum_2(E, V)]^{-1} \quad (5)$$

where the self-energy terms for electrodes 1 and 2 are

$$\sum_i(E, V) = (ES_{i\text{M}} - H_{i\text{M}})g_i(ES_{i\text{M}} - H_{i\text{M}}) \quad (6)$$

Here we are able to combine the continuous and discrete wave function in the same formalism.⁸² The transmission probability, T , and the total density of states, D , of the molecular junction are

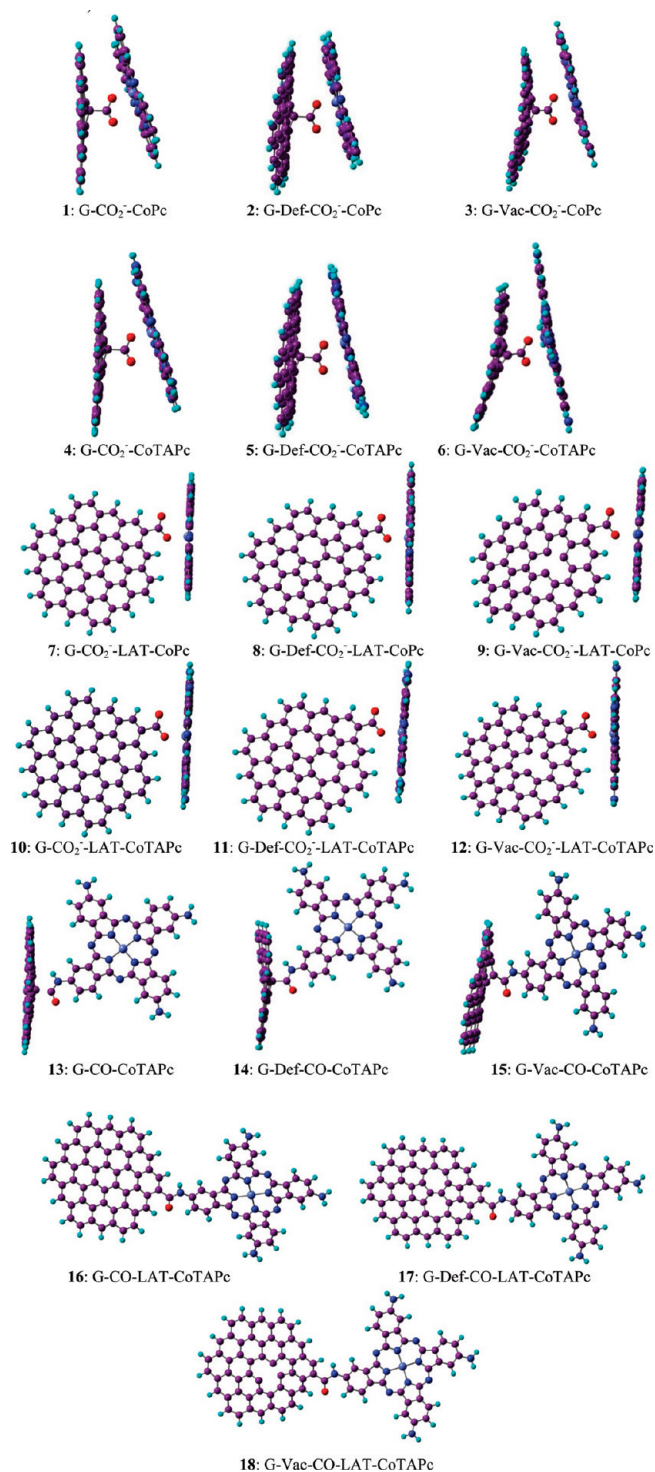


Figure 3. Optimized molecular structures of the 18 complexes calculated at B3LYP/6-31G/LANL2DZ level of theory.

calculated as follows:^{25,79,80}

$$T(E, V) = \text{Trace}(\Gamma_1(E, V)G_M(E, V)\Gamma_2(E, V)G_M^+(E, V)) \quad (7)$$

$$D(E, V) = \text{Trace}(i[G_M(E, V) - G_M^+(E, V)]S(V)) \quad (8)$$

Table 1. Optimized Geometrical Parameters Shown in Scheme 1^a

complex	R1	R2	D1
Cobalt-Centered Interaction			
1: G-CO ₂ ⁻ -CoPc	1.589	1.998	13.24
2: G-Def-CO ₂ ⁻ -CoPc	1.559	1.950	9.35
3: G-Vac-CO ₂ ⁻ -CoPc	1.467	1.908	15.27
4: G-CO ₂ ⁻ -CoTAPc	1.589	1.970	13.24
5: G-Def-CO ₂ ⁻ -CoTAPc	1.559	1.930	9.35
6: G-Vac-CO ₂ ⁻ -CoTAPc	1.467	1.890	15.27
7: G-CO ₂ ⁻ -LAT-CoPc	1.537	2.145	0.00
8: G-Def-CO ₂ ⁻ -LAT-CoPc	1.530	2.158	0.01
9: G-Vac-CO ₂ ⁻ -LAT-CoPc	1.535	2.144	6.22
10: G-CO ₂ ⁻ -LAT-CoTAPc	1.540	2.156	0.00
11: G-Def-CO ₂ ⁻ -LAT-CoTAPc	1.530	2.153	0.01
12: G-Vac-CO ₂ ⁻ -LAT-CoTAPc	1.538	2.156	6.22
complex	R3	R4	D2
Ligand-Centered Interaction			
13: G-CO-CoTAPc	1.658	1.359	13.28
14: G-Def-CO-CoTAPc	1.611	1.367	13.96
15: G-Vac-CO-CoTAPc	1.476	1.396	15.71
16: G-CO-LAT-CoTAPc	1.499	1.383	0.00
17: G-Def-CO-LAT-CoTAPc	1.496	1.382	0.02
18: G-Vac-CO-LAT-CoTAPc	1.500	1.383	4.81

^aDistances (\AA) and angles (degrees ($^\circ$)) for complexes calculated at the B3LYP/6-31G/LANL2DZ level of theory.

where $\Gamma_i = \sqrt{-1}(\Sigma_i(E, V)) - \Sigma_i^+(E, V)$ ($i, j = 1, 2$) describes the coupling between the contacts and the molecule, $S(V)$ is the overlap matrix at each applied voltage, G_M is the retarded Green function for the standalone molecule and G_M^+ is its adjoint.

Therefore the current is obtained from

$$I \approx \frac{2e}{h} \int_{E_f + V_1}^{E_f + V_2} T(E, V) dE \quad (9)$$

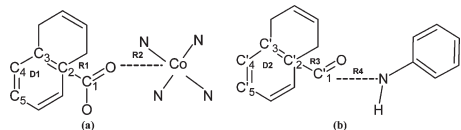
where e is the charge of the electron, h is Planck's constant, and E_f is the Fermi level of the molecular junction. Calculations for several kinds of systems has been performed in the past.^{71–73,78,83} The combined DFT-Green function formalism had been used by other groups to study the electron transport through organic molecules between gold electrodes, such as DNA,^{84,85} porphyrins,^{27,86} molecular wires,²⁸ molecular diodes and switches,^{24,28,87} and CNTs.¹¹

3. RESULTS AND DISCUSSION

Molecular Geometries. Molecular Geometries are optimized at the B3LYP/LANL2DZ/6-31G level of theory (Figure 3, Table 1, and Scheme 1). For all complexes, the functionalization by CO₂⁻ and CO on graphene is covalent as noted from the optimized distances R1 and R3 ranging from 1.5 to 1.6 \AA ; these distances are in agreement with typical single C–C bond distances of $\sim 1.54 \text{ \AA}$. The presence of defect and vacancy in graphene leads to a slight decrease in R1, in agreement with previous results reported for a similar graphene.⁴²

The adsorption of phthalocyanine (CoPc or CoTAPc) on the functionalized graphene is gauged by the optimized distance $r_{\text{Co}-\text{O}}$

Scheme 1. Geometrical Parameters for Complexes (a) 1–12 and (b) 13–18 Used in Table 1^a



^a R1 = $r_{C_2}-C_1$; R2 = r_{Co-O} ; R3 = $r_{C_2'-C_1'}$; R4 = $r_{C_1'-N}$; D1 = $\angle_{C_2C_3C_4C_5}$; D2 = $\angle_{C_2'C_3'C_4'C_5'}$.

(R2). For **1–6**, where the attachment with graphene– CO_2^- is through the cobalt atom, the deformation of pristine graphene (defect and vacancy) favors the adsorption of phthalocyanine, showing a shorter R2 of 1.95 and 1.91 Å, for **2** and **3** (G-Def and G-Vac, respectively, with CoPc), respectively, and 1.93 and 1.89 Å for **5** and **6** (now with CoTAPc), respectively, whereas for pristine graphene R2 is 1.99 Å for **1** (G with CoPc) and 1.97 Å for **4** (G with CoTAPc). When graphene functionalization is by the edge (**7–12**), phthalocyanine seems to be adsorbed on G- CO_2^- at slightly larger distances (~2.14 Å) than those for **1–6**. This is because van der Waals interactions between graphene- CO_2^- and CoPc (CoTAPc) in **1–6**; there, the parallel structure between the conjugated structures leads to a $\pi-\pi$ interaction, favoring shorter distances. Experimental bond lengths for cobalt–oxygen may vary depending of the type of structure; for instance in perovskite compounds, ($LaSrCoO_3$) r_{Co-O} values obtained by powder neutron diffraction data are in the range of 1.86–1.98 Å.⁸⁸ For dimer complexes of cobalt where the metal is pentacoordinated and each cobalt atom is bonded to two oxygen atoms, the X-ray diffraction method showed interatomic distances of Co–O covalent bond of 1.98 and 2.14 Å.¹⁸ These results suggest that complexes **1–6** and **7–12** might have a covalent character for the Co–O attachment.

The dihedral angle D1, characterizes the planarity degree of the graphene model. The results indicate that none of the graphenes in **1–6** are planar; they have a deviation out of the plane from 9 to 15°, being the largest in graphene with vacancy, because this structure has one less carbon atom, leading to a higher loss of hybridization. For **7, 8, 10**, and **11**, the graphene is completely planar ($D1 = 0^\circ$), but for the structures with vacancy, G-Vac (**9** and **12**) is ~6.2°; the loss of one carbon atom breaks the symmetry of graphene structure and leads the graphene out of the plane.

On the other hand, the attachment between G-CO and CoTAPc (**13–18**) by the substituent (NH_2) of the ligand shows shorter distances R4 (r_{C-N}), 1.36–1.38 Å, than R3, the distances of the two conjugated structures in **1–12** (attached through a Co–O); this is due mainly to the nature of the bond (C–N), suggesting a stronger interaction. These values are comparable to typical bonds C–N of acyclic amides (1.33 Å) obtained by X-ray and neutron diffraction.⁸⁹

We found nonplanar graphene structures for **13–15** characterized by a dihedral (Scheme 1) $D2 \approx 14^\circ$ that can be due to the position of CO functionalization, which is at the center of graphene, causing a slight deviation out of the plane, in the same way as **1–6**. The low electronic repulsion in G-CO-CoTAPc attachment in **16–18** yields a nearly coplanar structure; in addition, the graphene in **18** shows a nonplanar structure due to the vacancy.

Binding Energy. The adsorption of phthalocyanine structures on functionalized graphene is analyzed in terms of the binding

energy (E_{bind}) between them. We use the general form to calculate it, $E_{bind} = E(\text{complex}) - [E(\text{phthalocyanine}) + E(\text{functionalized-graphene})]$. The results for E_{bind} calculated using the B3PW91 functional are shown in Table 2.

Preliminary calculations with the B3LYP/6-31G/LANL2DZ level of theory showed differences for E_{bind} of ~2–49 kcal/mol. Thus, B3LYP without d functions in the basis set for first and second row atoms predicts lower binding energies in **13** of the 18 complexes; differences in absolute total energies calculated with both functionals are in the range of ~314–358 kcal/mol for the complexes and ~103–191 kcal/mol for the fragments. In order to validate our results of binding energy with these functionals, we did calculations on smaller molecules following the same methodology used here to get binding energy. Thus, the molecular geometry optimization is performed at the B3LYP/6-31G level of theory, and then self-consistent calculations with the B3PW91/6-31G(d) level of theory are performed. For instance, the binding energy of the OH group in methanol (CH_3OH) gave a difference between the two functionals of 3.8 kcal/mol and in phenol (C_6H_5OH) of 4.2 kcal/mol; in both cases B3LYP predicts higher stability, whereas the complex $CoH_2(OH)_2$ is less stable by 2.9 kcal/mol than when using the B3PW91 functional with d functions for the first and second row atoms. We conclude that the difference in E_{bind} obtained with these functionals depends strongly on the structure size; in our case, the complex shows that the only explanation for such huge differences in E_{bind} is the importance that electronic correlation has in those structures. B3LYP and B3PW91 differ only on the correlation functional; however, the effect of the polarization functions does not allow us to separate the functional effects in the binding energies.

Overall, we find good agreement between the results from the two functionals predicting the most stable complex, which correspond to those whose graphene has a defect or vacancy. In particular, we found that for **1–12**, graphene functionalized with CO_2^- -B3LYP functional suggests that the complexes with CoPc are more stable than those with CoTAPc by 10 kcal/mol, though B3PW91 functional shows higher stability (~20 kcal/mol) for complexes with CoTAPc instead of CoPc. In the case of **13–18** (graphene functionalized with CO), both functionals follow the same trend; the most stable complexes correspond to structures fully coplanar (**16–18**) and no interaction between the conjugates takes place.

From now on, we will focus on the results gotten with B3PW91/6-31G(d)/LANL2DZ in order to be consistent with the current–voltage analysis performed with the same functional that has been evidenced to be enough for this kind of analysis.^{22,30,34,35,78–80}

The structural conformations of the complexes are very different and consequently their binding energies too. We analyze two types of graphene structures for complexes with cobalt-centered attachments: parallel and perpendicular. Among the complexes with parallel structures (**1–6**), only those with CoTAPc (**4–6**) show to be stable as confirmed by their negative binding energies. However, complexes with perpendicular structures (**7–12**) are all stable, with **10–12** the most stable ($E_{bind} \approx -20$ kcal/mol); this could be explained by the R2 distances r_{Co-O} (~2.15 Å) in **7–12** that are larger than the corresponding lengths (~1.94 Å) in structures of parallel structure, **1–6**, where the electronic repulsion between G- CO_2^- and CoPc (CoTAPc) π -clouds is higher. For complexes with ligand-centered attachment, **13–18**, the B3PW91 functional yields a

Table 2. Total (E) and Binding (E_{bind}) Energies, Electrical Dipole Moment (p), HOMO, LUMO, and HOMO-LUMO Gap Energies for All of the Complexes at the B3PW91/6-31G(d)/LANL2DZ Level of Theory

complex	E (Ha)	E_{bind} (kcal/mol)	p (D)	HOMO (eV)	LUMO (eV)	HLG (eV)
1: G-CO ₂ ⁻ -CoPc	-4068.314409	14.06	1.92	-1.61	-0.60	1.00
2: G-Def-CO ₂ ⁻ -CoPc	-4068.212590	13.21	4.09	-1.82	-0.86	0.96
3: G-Vac-CO ₂ ⁻ -CoPc	-4030.049268	13.19	4.47	-1.70	-0.78	0.91
4: G-CO ₂ ⁻ -CoTAPc	-4289.635052	-5.36	4.27	-1.35	-0.31	1.03
5: G-Def-CO ₂ ⁻ -CoTAPc	-4289.535538	-7.65	6.29	-1.56	-0.55	1.01
6: G-Vac-CO ₂ ⁻ -CoTAPc	-4251.372600	-8.02	6.60	-1.44	-0.49	0.96
7: G-CO ₂ ⁻ -LAT-CoPc	-4067.834736	-1.28	9.22	-2.70	-0.52	2.18
8: G-Def-CO ₂ ⁻ -LAT-CoPc	-4067.704898	-0.64	8.82	-2.73	-0.94	1.79
9: G-Vac-CO ₂ ⁻ -LAT-CoPc	-4029.448317	-1.50	9.86	-2.68	-1.28	1.40
10: G-CO ₂ ⁻ -LAT-CoTAPc	-4289.153950	-19.80	7.21	-2.09	-0.42	1.67
11: G-Def-CO ₂ ⁻ -LAT-CoTAPc	-4289.025235	-19.86	6.89	-2.10	-0.83	1.27
12: G-Vac-CO ₂ ⁻ -LAT-CoTAPc	-4250.767105	-19.75	7.91	-2.07	-1.17	0.89
13: G-CO-CoTAPc	-4213.747584	25.24	3.65	-4.01	-3.74	0.27
14: G-Def-CO-CoTAPc	-4213.645532	13.48	6.23	-4.27	-3.98	0.30
15: G-Vac-CO-CoTAPc	-4175.494211	7.42	2.18	-4.31	-3.84	0.48
16: G-CO-LAT-CoTAPc	-4213.241524	-107.54	4.49	-4.05	-2.37	1.67
17: G-Def-CO-LAT-CoTAPc	-4213.156131	-135.89	5.07	-4.49	-2.78	1.70
18: G-Vac-CO-LAT-CoTAPc	-4174.902631	-135.87	4.81	-4.47	-3.12	1.35

higher stability for **16–18** because of the lower electronic repulsion between graphene and phthalocyanine when they are coplanar and also because the highest stability is found for complexes with vacancy and defect on graphene, **17–18**, with $E_{\text{bind}} \approx -135$ kcal/mol.

B3PW91 functional predicts that complexes **13–15** would not be formed because of their positive binding energy values. However, structures **16–18** have been synthesized for graphene oxide linked to porphyrin through an amide bond CO-NH^{19,37} that could explain the higher stability that these complexes have with respect to the others studied in this work.

Molecular Orbital. Molecular orbital energies, HOMO and LUMO and the energy gap (HLG), calculated with the B3PW91 functional are shown in Table 2, and their molecular surfaces are shown in Figure 4, including a picture of the energy levels for 30 occupied and virtual molecular orbitals.

We noticed that the perturbation on graphene, G-Def, and G-Vac, produces a stabilization of the frontier molecular orbitals of up to 0.5 eV for HOMO and 0.8 eV for LUMO. The behavior is different for the HLG, for instance, in complexes with cobalt-centered attachment (**1–12**), HLG decreases for complexes with G-Def and G-Vac in comparison with pristine graphene. This means that from the molecular orbital viewpoint **1, 4, 7, and 10** are less reactive to electron transfer. In the case of the complexes with ligand-centered attachment (**13–18**), with exception of **18**, the opposite is observed, HLG increases for complexes with G-Def and G-Vac, indicating that the perturbation on the graphene structure leads to a reduction of electronic reactivity.

We also find that when graphene is functionalized with CO₂⁻ at the edge (**7–12**), with the exception of **12**, the attachment with CoPc (CoTAPc) is preferred, as suggested by a larger HLG, in comparison to the structures with CO₂⁻ functionalized at the center of graphene (**1–6**). This can be understood in terms of the reduced electronic repulsion between the conjugated structures, G-CoPc (CoTAPc), in **7–11**, which have perpendicular structure rather than parallel as in **1–6**.

On the other hand, HOMO and LUMO surfaces are shown to be dependent on the conformation of the conjugated structures. Parallel structures (**1–6**) show high participation of graphene in both molecular orbitals with a contribution of cobalt atom in the phthalocyanine. Perpendicular structures (**7–12**) show that their HOMO is localized on the phthalocyanine ligand (no metal) and the LUMO on the graphene, suggesting that in these complexes, CoPc (CoTAPc) is an electron donor species and the graphene is an electron withdrawing one. This suggests a charge transfer from the HOMO to the LUMO and therefore a change of electronic density from phthalocyanine to graphene. This feature of graphene to increase its electronic charge induced by other molecule, makes it a potential resistance-based sensor, thus it could be also used as phthalocyanine sensor.

Complexes **13–15** show similar HOMO and LUMO, which are mainly localized on the graphene and cobalt with a minor contribution in the phthalocyanine ligand. No meaningful changes are seen between both molecular orbitals for **13** and **14**, but for **15**, a higher contribution in the LUMO of phthalocyanine ligand (in the C–N of the G-CoTAPc linking) is observed.

Meanwhile **16–18** show a similar behavior to **7–12**; their HOMOs are localized in phthalocyanine ligand, with a contribution from the cobalt to the HOMO in **16** and the LUMOs are on the graphene; therefore, complexes **16–18** might show electron transfer from phthalocyanine HOMO to graphene LUMO. Thus, similarly to **7–12**, they could be used as charge-transfer sensors. For these complexes (**7–12** and **16–18**), although their LUMO are on the graphene, it is clear for the complexes with G-Vac (**9, 12, and 18**) that their LUMO's are mostly localized in the vacancy rather than delocalized over the graphene, suggesting a reduced electron transfer. However, the structure of phthalocyanine with respect to graphene could affect the amount of current.

After the analysis of the frontier molecular orbitals, and considering they are in both conjugates, we can understand why the HLG of **1–6** is smaller than the HLG of **7–12**, when

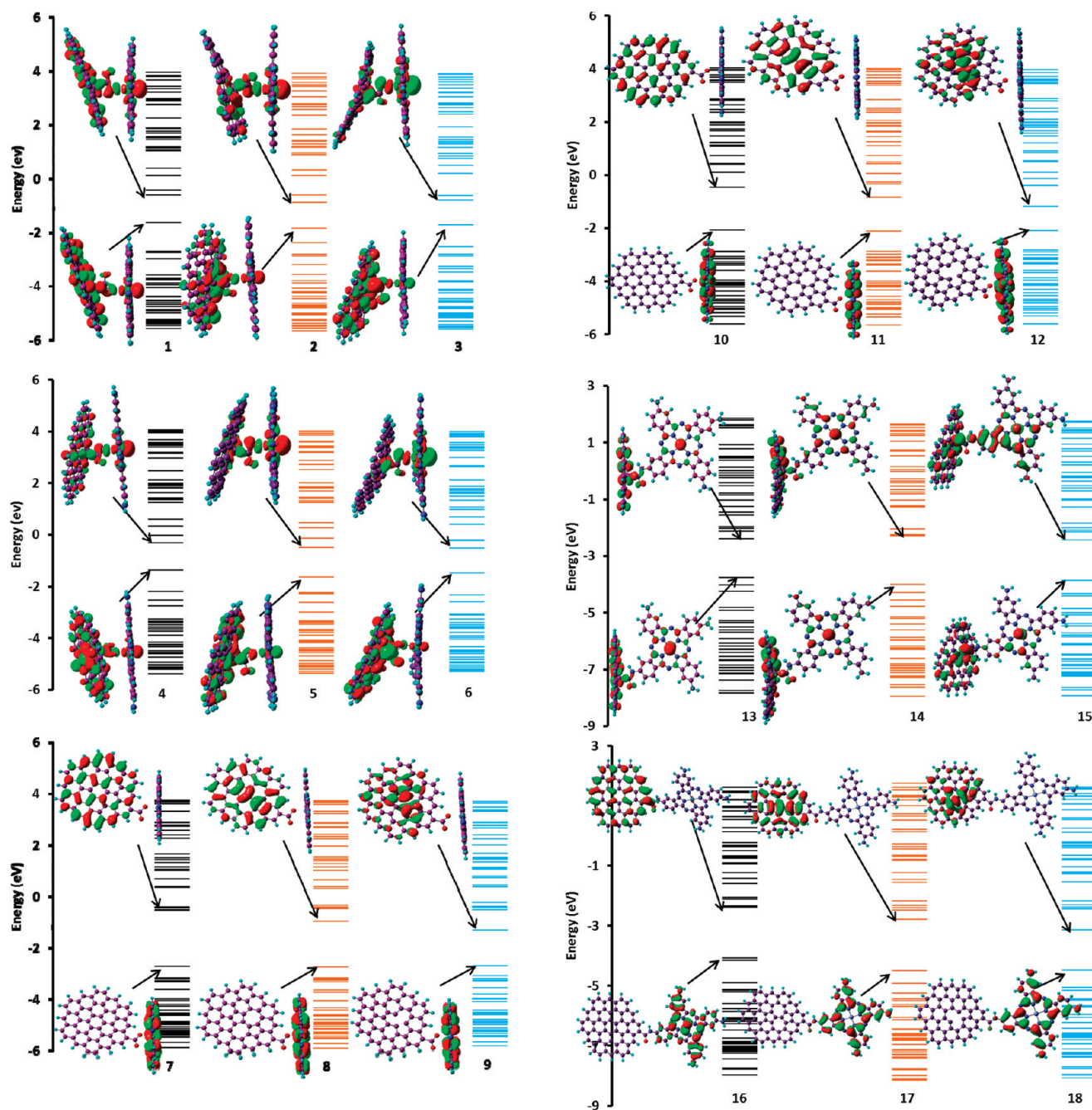


Figure 4. Molecular orbitals of the complexes calculated at the B3PW91/6-31G(d)/LANL2DZ level of theory. G (black), G-Def (orange), and G-Vac (light blue). Isosurfaces of the LUMO (top) and HOMO (bottom) are also included.

both have CO_2^- functionalization; this is because the conjugated structures in **1–6** are facing in parallel structure favoring charge transfer between the π clouds.

Current–Voltage Analysis. Current–voltage analysis of the complexes obtained through DFT-Green's function calculations are showed in Figure 5; the results are shown by complex conformations and phthalocyanine model, and the influence of each graphene model (G, G-Def, G-Vac) is compared. For all complexes, we applied positive bias in a way that current from phthalocyanine to graphene is induced, $\text{CoPc}(\text{CoTAPc}) \rightarrow \text{G}$; the current is calculated at -1 (negative bias), 0 , and $+1$ V (positive bias).

For parallel structures, cobalt-centered complexes (G-CO_2^- center functionalization) (**1–6**), the standard current (defined for positive charges) is asymmetric in both directions, higher in the direction of $\text{CoPc}(\text{CoTAPc}) \rightarrow \text{G}$ for complexes with pristine graphene (**1** and **4**) and G-Def (**2** and **5**), whereas it is higher in the opposite direction, $\text{G} \rightarrow \text{CoPc}(\text{CoTAPc})$, for complexes with G-Vac (**3** and **6**). Complexes with pristine graphene (**1** and **4**) show higher current than those with G-Def (**2** and **5**) and G-Vac (**3** and **6**), despite the fact that **1** and **4** have larger HLGs. For **1** and **4** the effect of the amine groups (NH_2) is large as substituent in the phthalocyanine ligand, because it causes a decrease in the current, for instance, the currents in **1** are -3.88 and $+7.40 \mu\text{A}$

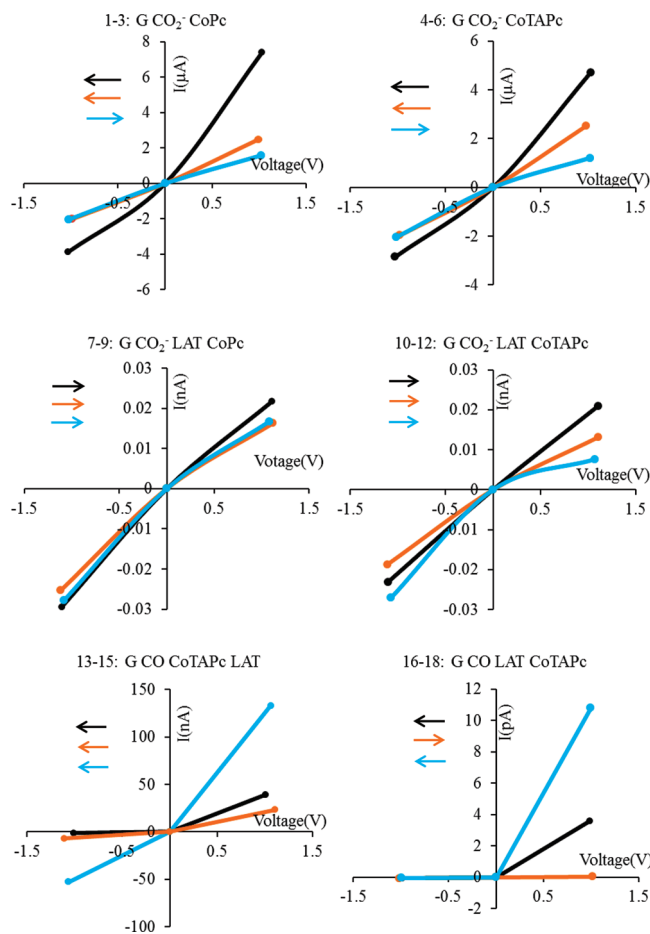


Figure 5. Current–voltage characteristics of complexes G-CoPc (CoTAPc). The arrows indicate the preferred current direction. According to the conjugates position in Figure 3, at positive (direct) bias the current is from CoPc (CoTAPc) to G (\leftarrow). Color curves relate to graphene models in complexes: G (black), G-Def (orange), and G-Vac (light blue). Calculated points are interconnected to help the eye.

and for **4** are -2.85 and $+4.71 \mu\text{A}$ for voltages different from zero, in which HLG for **1** is 0.03 eV smaller than the gap in **4**.

For perpendicular structures, cobalt-centered complexes (G-CO₂⁻ edge functionalization) (**7–12**), the conduction is remarkably lower when compared to complexes with parallel structures (**1–6**) due to the arrangement of the conjugated structures G and CoPc (CoTAPc), where the connection is just through a linking bond, and thus the current is small. Though there is conduction in both directions, the current is slightly higher from G \rightarrow CoPc (CoTAPc); which is in agreement with their frontier orbitals. Having the HOMO in CoPc (CoTAPc) and the LUMO in G suggests an easy way for the electrons to be carried from CoPc (CoTAPc) to G; however, at a higher bias, the complexes with G, G-Def, and G-Vac show similar values of current. Also, as it takes place in **1** and **4**, we found **7** (-0.03 nA) showing a slightly higher current than **10** (-0.02 nA), at $\sim 1 \text{ V}$, despite the fact that the HLG of **7** (2.18 eV) is larger, and the same trend is observed between those with defect and vacancy; complexes with CoPc feature higher current.

In the case of CO functionalized complexes, **13–18**, we notice a difference in the electric conduction for perpendicular and coplanar structures. For **13–15** the currents are shifted in the

direction CoTAPc \rightarrow G and remarkably the highest conduction is observed for the complex with G-Vac **15** ($+0.1 \mu\text{A}$ at 1 V). This can be due to its HOMO having more contribution in G-CO bonding and also because the LUMO has more contribution in the attachment region G-CoTAPc (C–N bond) than the LUMOs of **13** and **14**. The conduction increases for complex **15** despite the fact that it has a larger HLG than pristine graphene **13**.

We notice that the complexes functionalized with CO, **13–15**, show higher currents than complexes functionalized with CO₂⁻ (**10–12**, even **7–9**) when both conformations have G-CoTAPc attachment and perpendicular structure. Complexes **10–12** have the perpendicular structure of graphene and the linking is through (Co–O), whereas **13–15** have the perpendicular structure of phthalocyanine (CoTAPc), and the link is through (C–N), that being the latter link in order to better achieve higher currents, in addition to the fact that these complexes (**13–15**) show smaller HLG.

The coplanar structure of complexes **16–18** is not strictly planar, and that fact can affect the current, which is lower (by $\sim 0.01 \text{ nA}$) than **13–15**, and again the higher conduction takes place in the complex with G-Vac (**18**) in similar fashion to **15**. A characteristic of complexes **13–18**, but not **17**, is that the conduction is not symmetric in both directions, resembling a diode behavior, and it is larger for the direction CoTAPc \rightarrow G. Complex **17** has the smallest current (and HLG larger than **16**), and it is on the order of 0.01 pA at both positive and negative bias.

4. CONCLUSIONS

We investigate, using a combined DFT and Green's function approach (GENIP) at the B3PW91/6-31G(d)/LANL2DZ(Co) level of theory, the electric characteristics of complexes of cobalt-phthalocyanine (CoPc, CoTAPc) adsorbed on graphene functionalized with CO₂⁻ or CO. Three models of graphene are used, pristine, defect, and vacancy, leading to a total of 18 complexes. Twelve of them are built with CO₂⁻ functionalization (**1–12**), and the remaining six (**13–18**) are built with CO functionalization. The functionalization arrangement, either at the center or at the periphery of graphene leads to parallel, perpendicular, and coplanar structures with respect to the phthalocyanine, resulting in changes of their individual molecular and electronic properties.

Overall, we found that complexes carrying a graphene with a defect or vacancy are of higher stability than pristine graphene. Binding energy calculations for the attachment between graphene and phthalocyanine show larger stability of formation (-100 to -130 kcal/mol) for complexes having a graphene-CO attached to phthalocyanine by an amide bond (complexes **16–18**), where the conjugated structures (graphene and phthalocyanine) have a coplanar structure. The formation of complexes with functionalization CO₂⁻ in graphene (negative values in binding energy) occurs but preferably when it is involved with CoTAPc (**10–12**) (-20 kcal/mol). The calculations of the optimized geometry performed at the B3LYP/6-31G/LANL2DZ-(Co) level of theory predict an adsorption distance Co–O of 1.9 – 2.1 \AA for complexes G-CO₂⁻ and C–N of $\sim 1.4 \text{ \AA}$ for complexes G-CO; according to the literature they are considered covalent distances.

The frontier molecular orbital, HOMO and LUMO, shapes suggest that 9 of the complexes (**7–12** and **16–18**) transfer charge from phthalocyanine to graphene; thus, they could be

used as phthalocyanine sensors, taking advantage of the absorption properties of the phthalocyanine in the UV-vis region.

The calculations of the current showed that the conduction is preferably favored in complexes with parallel structure (**1–6**), with currents of up to $\sim 7 \mu\text{A}$, and functionalization CO_2^- , where both conjugated structures are facing each other, thus favoring an increase of current through their $\pi-\pi$ bridge. The conduction is very poor for the complexes of higher stability (**10–12** and **16–18**) and those with charge transfer processes (**7–9**), having perpendicular or coplanar structures.

Complexes with G-CO functionalization, **13–15**, yield higher currents than those with G- CO_2^- functionalization, **10–12**, and even higher than the current in complexes **7–9**. Since the attachment between conjugated structures is through the covalent bonds Co–O in **7–12** and C–N in **13–15**, we conclude that C–N attachment is better for electron transfer between the conjugates.

ACKNOWLEDGMENT

We acknowledge financial support from the U.S. Defense Threat Reduction Agency DTRA through the U.S. Army Research Office, Project No. W91NF-06-1-0231, ARO/DURINT Project No. W91NF-07-1-0199, and ARO/MURI Project No. W91NF-11-1-0024 as well as from the Department of Energy/Basic Energy Sciences (DE-FG02-05ER15729). G.I.C.J. acknowledges CONICYT/CHILE, Project FONDECYT #1090700 and DICYT/USACH for financial support for a research stay at Texas A&M University. We also thank DICYT/USACH, Project Complementary Support, for computational time provided. D.C.A. thanks CONICYT for a doctoral fellowship.

REFERENCES

- (1) Novoselov, K. S.; Geim, A. K.; Morozov, S. V.; Jiang, D.; Zhang, Y.; Dubonos, S. V.; Grigorieva, I. V.; Firsov, A. A. Electric field effect in atomically thin carbon films. *Science* **2004**, *306*, 666.
- (2) Soldano, C.; Mahmood, A.; Dujardin, E. Production, properties and potential of graphene. *Carbon* **2010**, *48*, 2127.
- (3) Subrahmanyam, K. S.; Vivekchand, S. R. C.; Govindaraj, A.; Rao, C. N. R. A study of graphenes prepared by different methods: characterization, properties and solubilization. *J. Mater. Chem.* **2008**, *18*, 1517.
- (4) Novoselov, K. S.; Geim, A. K.; Morozov, S. V.; Jiang, D.; Katsnelson, M. I.; Grigorieva, I. V.; Dubonos, S. V.; Firsov, A. A. Two-dimensional gas of massless Dirac fermions in graphene. *Nature* **2005**, *438*, 197.
- (5) Dikin, D. A.; Stankovich, S.; Zimney, E. J.; Piner, R. D.; Dommett, G. H. B.; Evmenenko, G.; Nguyen, S. T.; Ruoff, R. S. Preparation and characterization of graphene oxide-based paper. *Nature* **2007**, *448*, 457.
- (6) Schedin, F.; Geim, A. K.; Morozov, S. V.; Hill, E. W.; Blake, P.; Katsnelson, M. I.; Novoselov, K. S. Detection of individual gas molecules adsorbed on graphene. *Nat. Mater.* **2007**, *6*, 652.
- (7) Meyer, J. C.; Geim, A. K.; Katsnelson, M. I.; Novoselov, K. S.; Booth, T. J.; Roth, S. The structure of suspended graphene sheets. *Nature* **2007**, *446*, 60.
- (8) Seminario, J. M.; Yan, L.; Ma, Y. Scenarios for Molecular-Level Signal Processing. *Proc. IEEE* **2005**, *93*, 1753.
- (9) Popov, V. N.; Henrard, L.; Lambin, P. Resonant Raman spectra of graphene with point defects. *Carbon* **2009**, *47*, 2448.
- (10) Kang, J.; Bang, J.; Ryu, B.; Chang, K. J. Effect of atomic-scale defects on the low-energy electronic structure of graphene: Perturbation theory and local-density-functional calculations. *Phys. Rev. B* **2008**, *77*, 115453.
- (11) Kang, Y.-J.; Kim, Y.-H.; Chang, K. J. Electrical transport properties of nanoscale devices based on carbon nanotubes. *Curr. Appl. Phys.* **2009**, *9*, S7.
- (12) Carlsson, J. M.; Scheffler, M. Structural, Electronic, and Chemical Properties of Nanoporous Carbon. *Phys. Rev. Lett.* **2006**, *96*, 046806.
- (13) Boukhvalov, D. W.; Katsnelson, M. I. Chemical Functionalization of Graphene with Defects. *Nano Lett.* **2008**, *8*, 4373.
- (14) Compton, O. C.; Dikin, D. A.; Putz, K. W.; Brinson, L. C.; Nguyen, S. T. Electrically Conductive “Alkylated” Graphene Paper via Chemical Reduction of Amine-Functionalized Graphene Oxide Paper. *J. Adv. Mater.* **2010**, *22*, 892.
- (15) Frisch, M. J.; Trucks, G. W.; Schlegel, H. B.; Scuseria, G. E.; Robb, M. A.; Cheeseman, J. R.; Scalmani, G.; Barone, V.; Mennucci, B.; Petersson, G. A.; Nakatsuji, H.; Caricato, M.; Li, X.; Hratchian, H. P.; Izmaylov, A. F.; Bloino, J.; Zheng, G.; Sonnenberg, J. L.; Hada, M.; Ehara, M.; Toyota, K.; Fukuda, R.; Hasegawa, J.; Ishida, M.; Nakajima, T.; Honda, Y.; Kitao, O.; Nakai, H.; Vreven, T.; Montgomery, J., J., A.; Peralta, J. E.; Ogliaro, F.; Bearpark, M.; Heyd, J. J.; Brothers, E.; Kudin, K. N.; Staroverov, V. N.; Kobayashi, R.; Normand, J.; Raghavachari, K.; Rendell, A.; Burant, J. C.; Iyengar, S. S.; Tomasi, J.; Cossi, M.; Rega, N.; Millam, N. J.; Klene, M.; Knox, J. E.; Cross, J. B.; Bakken, V.; Adamo, C.; Jaramillo, J.; Gomperts, R.; Stratmann, R. E.; Yazyev, O.; Austin, A. J.; Cammi, R.; Pomelli, C.; Ochterski, J. W.; Martin, R. L.; Morokuma, K.; Zakrzewski, V. G.; Voth, G. A.; Salvador, P.; Dannenberg, J. J.; Dapprich, S.; Daniels, A. D.; Farkas, Ö.; Foresman, J. B.; Ortiz, J. V.; Cioslowski, J.; Fox, D. J.; Gaussian 09, revision A.02; Gaussian, Inc.: Wallingford, CT, 2009.
- (16) Ma, J.; Alfograve, D.; Michaelides, A.; Wang, E. Stone-Wales defects in graphene and other planar sp²-bonded materials. *Phys. Rev. B* **2009**, *80*, 033407.
- (17) Mao, J.; Zhang, H.; Jiang, Y.; Pan, Y.; Gao, M.; Xiao, W.; Gao, H. J. Tunability of Supramolecular Kagome Lattices of Magnetic Phthalocyanines Using Graphene-Based Moiré Patterns as Templates. *J. Am. Chem. Soc.* **2009**, *131*, 14136.
- (18) Sarkar, M.; Clérac, R.; Mathonière, C.; Hearns, N. G. R.; Bertolasi, V.; Ray, D. Azido, Cyanato, and Thiocyanato Coordination Induced Distortions in Pentacoordinated [CoIIA(bip)]₂ (A = NCS⁻, N³⁻, or NCO⁻) Complexes. *Eur. J. Inorg. Chem.* **2009**, *2009*, 4675.
- (19) Xu, Y.; Liu, Z.; Zhang, X.; Wang, Y.; Tian, J.; Huang, Y.; Ma, Y.; Zhang, X.; Chen, Y. A Graphene Hybrid Material Covalently Functionalized with Porphyrin: Synthesis and Optical Limiting Property. *Adv. Mater.* **2009**, *21*, 1275.
- (20) Wei, D.; Liu, Y.; Wang, Y.; Zhang, H.; Huang, L.; Yu, G. Synthesis of N-Doped Graphene by Chemical Vapor Deposition and Its Electrical Properties. *Nano Lett.* **2009**, *9*, 1752.
- (21) An, W.; Wu, X.; Yang, J. L.; Zeng, X. C. Adsorption and Surface Reactivity on Single-Walled Boron Nitride Nanotubes Containing Stone-Wales Defects. *J. Phys. Chem. C* **2007**, *111*, 14105.
- (22) Bautista, E. J.; Yan, L.; Seminario, J. M. Ab initio analysis of electron transport in oligoglycines. *J. Phys. Chem. C* **2007**, *111*, 14552.
- (23) Frisch, M. J.; Trucks, G. W.; Schlegel, H. B.; Scuseria, G. E.; Robb, M. A.; Cheeseman, J. R.; Montgomery, J. A.; Vreven, J. T.; Kudin, K. N.; Burant, J. C.; Millam, J. M.; Iyengar, S. S.; Tomasi, J.; Barone, V.; Mennucci, B.; Cossi, M.; Scalmani, G.; Rega, N.; Petersson, G. A.; Nakatsuji, H.; Hada, M.; Ehara, M.; Toyota, K.; Fukuda, R.; Hasegawa, J.; Ishida, M.; Nakajima, T.; Honda, Y.; Kitao, O.; Nakai, H.; Klene, M.; Li, X.; Knox, J. E.; Hratchian, H. P.; Cross, J. B.; Bakken, V.; Adamo, C.; Jaramillo, J.; Gomperts, R.; Stratmann, R. E.; Yazyev, O.; Austin, A. J.; Cammi, R.; Pomelli, C.; Ochterski, J. W.; Ayala, P. Y.; Morokuma, K.; Voth, G. A.; Salvador, P.; Dannenberg, J. J.; Zakrzewski, V. G.; Dapprich, S.; Daniels, A. D.; Strain, M. C.; Farkas, O.; Malick, D. K.; Rabuck, A. D.; Raghavachari, K.; Foresman, J. B.; Ortiz, J. V.; Cui, Q.; Baboul, A. G.; Clifford, S.; Cioslowski, J.; Stefanov, B. B.; Liu, G.; Liashenko, A.; Piskorz, P.; Komaromi, I.; Martin, R. L.; Fox, D. J.; Keith, T.; Al-Laham, M. A.; Peng, C. Y.; Nanayakkara, A.; Challacombe, M.; Gill, P. M. W.; Johnson, B.; Chen, W.; Wong, M. W.; Gonzalez, C.; Pople, J. A.; Gaussian 03, revision E.01; Gaussian, Inc.: Wallingford, CT, 2007.

- (24) Ganji, M. D.; Nourozi, F. Density functional non-equilibrium Green's function (DFT-NEGF) study of the smallest nano-molecular switch. *Physica E* **2008**, *40*, 2606.
- (25) Sotelo, J. C.; Seminario, J. M. Biatom substrates for bulk-molecule interfaces: The PtCo-oxygen interface. *J. Chem. Phys.* **2007**, *127*, 244706 (13 pp).
- (26) Sotelo, J. C.; Yan, L.; Wang, M.; Seminario, J. M. Field Induced Conformational Changes in Bimetallic Oligoaniline Junctions. *Phys. Rev. A* **2007**, *75*, 022511.
- (27) Yanov, I.; Kholod, Y.; Leszczynski, J.; Palacios, J. J. Electron transport properties of the porphyrin molecule located between gold electrodes. *Chem. Phys. Lett.* **2007**, *445*, 238.
- (28) Aghaie, H.; Gholami, M. R.; Monajjemi, M.; Ganji, M. D. Electron transport phenomenon simulation through the carborane nano-molecular wire. *Physica E* **2008**, *40*, 2965.
- (29) Li, Y.; Zhou, Z.; Golberg, D.; Bando, Y.; Schleyer, P. v. R.; Chen, Z. Stone-Wales Defects in Single-Walled Boron Nitride Nanotubes: Formation Energies, Electronic Structures, and Reactivity. *J. Phys. Chem. C* **2008**, *112*, 1365.
- (30) Cristancho, D.; Seminario, J. M. Polypeptides in alpha-helix conformation perform as diodes. *J. Chem. Phys.* **2010**, *132*.
- (31) Hu, Y.; Shen, J.; Li, N.; Shi, M.; Ma, H.; Yan, B.; Wang, W.; Huang, W.; Ye, M. Amino-functionalization of graphene sheets and the fabrication of their nanocomposites. *Polym. Compos.* **2010**, *31*, 1987.
- (32) Ma, K. L.; Yan, X. H.; Xiao, Y.; Chen, Y. P. Electronic transport properties of metallic graphene nanoribbons with two vacancies. *Solid State Commun.* **2010**, *150*, 1308.
- (33) Padilha, J. E.; Amorim, R. G.; Rocha, A. R.; da Silva, A. J. R.; Fazzio, A. Energetics and stability of vacancies in carbon nanotubes. *Solid State Commun.* **2011**, *151*, 482.
- (34) Rangel, N. L.; Seminario, J. M. Single molecule detection using graphene electrodes. *J. Phys. B: At., Mol. Opt. Phys.* **2010**, *43*, 115101.
- (35) Rangel, N. L.; Seminario, J. M. Vibronics and plasmonics based graphene sensors. *J. Chem. Phys.* **2010**, *132*, 125102.
- (36) Kamat, P. V. Graphene-Based Nanoassemblies for Energy Conversion. *J. Phys. Chem. Lett.* **2011**, *2*, 242.
- (37) Yang, H.; Shan, C.; Li, F.; Han, D.; Zhang, Q.; Niu, L. Covalent functionalization of polydisperse chemically-converted graphene sheets with amine-terminated ionic liquid. *Chem. Commun.* **2009**, 3880.
- (38) Chunder, A.; Pal, T.; Khondaker, S. I.; Zhai, L. Reduced Graphene Oxide/Copper Phthalocyanine Composite and Its Optoelectrical Properties. *J. Phys. Chem. C* **2010**, *114*, 15129.
- (39) Huang, K.-J.; Niu, D.-J.; Sun, J.-Y.; Han, C.-H.; Wu, Z.-W.; Li, Y.-L.; Xiong, X.-Q. Novel electrochemical sensor based on functionalized graphene for simultaneous determination of adenine and guanine in DNA. *Colloids Surf., B* **2011**, *82*, 543.
- (40) Akhavan, O. Photocatalytic reduction of graphene oxides hybridized by ZnO nanoparticles in ethanol. *Carbon* **2011**, *49*, 11.
- (41) Park, J. S.; Cho, S. M.; Kim, W.-J.; Park, J.; Yoo, P. J. Fabrication of Graphene Thin Films Based on Layer-by-Layer Self-Assembly of Functionalized Graphene Nanosheets. *ACS Appl. Mater. Interfaces* **2011**, *3*, 360.
- (42) Al-Aqtash, N.; Vasiliev, I. Ab Initio Study of Carboxylated Graphene. *J. Phys. Chem. C* **2009**, *113*, 12970.
- (43) Stone, A. J.; Wales, D. J. Theoretical studies of icosahedral C₆₀ and some related species. *Chem. Phys. Lett.* **1986**, *128*, 501.
- (44) Becke, A. D. Density-functional thermochemistry. III. The role of exact exchange. *J. Chem. Phys.* **1993**, *98*, 5648.
- (45) Becke, A. D. Density-functional exchange-energy approximation with correct asymptotic behavior. *Phys. Rev. A* **1988**, *38*, 3098.
- (46) Lee, C.; Yang, W.; Parr, R. G. Development of the Colle-Salvetti correlation-energy formula into a functional of the electron density. *Phys. Rev. B* **1988**, *37*, 785.
- (47) Miehlich, B.; Savin, A.; Stoll, H.; Preuss, H. Results obtained with the correlation-energy density functionals of Becke and Lee, Yang and Parr. *Chem. Phys. Lett.* **1989**, *157*, 200.
- (48) Hehre, W. J.; Ditchfield, R.; Pople, J. A. Self-Consistent Molecular Orbital Methods. XII. Further Extensions of Gaussian-Type Basis Sets for Use in Molecular Orbital Studies of Organic Molecules. *J. Chem. Phys.* **1972**, *56*, 2257.
- (49) Hay, P. J.; Wadt, W. R. Ab initio effective core potentials for molecular calculations - potentials for the transition-metal atoms Sc to Hg. *J. Chem. Phys.* **1985**, *82*, 270.
- (50) Hay, P. J.; Wadt, W. R. Ab initio effective core potentials for molecular calculations - potentials for K to Au including the outermost core orbitals. *J. Chem. Phys.* **1985**, *82*, 299.
- (51) Wadt, W. R.; Hay, P. J. Ab initio effective core potentials for molecular calculations - potentials for main group elements Na to Bi. *J. Chem. Phys.* **1985**, *82*, 284.
- (52) Perdew, J. P. Unified Theory of Exchange and Correlation beyond the Local Density Approximation. In *Electronic Structure of Solids*; Ziesche, P., Eschrig, H., Eds.; Akademie Verlag: Berlin, 1991; p 11.
- (53) Perdew, J. P.; Chevary, J. A.; Vosko, S. H.; Jackson, K. A.; Pederson, M. R.; Singh, D. J.; Fiolhais, C. Atoms, Molecules, Solids, and Surfaces: Applications of the Generalized Gradient Approximation for Exchange and Correlation. *Phys. Rev. B* **1992**, *46*, 6671.
- (54) Perdew, J. P.; Chevary, J. A.; Vosko, S. H.; Jackson, K. A.; Pederson, M. R.; Singh, D. J.; Fiolhais, C. Atoms, Molecules, Solids, and Surfaces - Applications of the Generalized Gradient Approximation for Exchange and Correlation *Phys. Rev. B* **1992**, *46*, 6671. *Phys Rev B* **1993**, *48*, 4978.
- (55) Perdew, J. P.; Burke, K.; Wang, Y. Generalized gradient approximation for the exchange-correlation hole of a many-electron system. *Phys. Rev. B* **1996**, *54*, 16533.
- (56) Burke, K.; Perdew, J. P.; Wang, Y. Derivation of a generalized gradient approximation: The PW91 density functional. In *Electronic Density Functional Theory: Recent Progress and New Directions*; Dobson, J. F., Vignale, G., Das, M. P., Eds.; Plenum: New York, 1997.
- (57) Petersson, G. A.; Bennett, A.; Tensfeldt, T. G.; Al-Laham, M. A.; Shirley, W. A.; Mantzaris, J. A complete basis set model chemistry. I. The total energies of closed-shell atoms and hydrides of the first-row elements. *J. Chem. Phys.* **1988**, *89*, 2193.
- (58) Petersson, G. A.; Al-Laham, M. A. A complete basis set model chemistry. II. Open-shell systems and the total energies of the first-row atoms. *J. Chem. Phys.* **1991**, *94*, 6081.
- (59) Balbuena, P. B.; Altomare, D.; Agapito, L. A.; Seminario, J. M. Theoretical analysis of Oxygen adsorption on Pt-based clusters alloyed with Co, Ni, or Cr embedded in a Pt matrix. *J. Phys. Chem. B* **2003**, *107*, 13671.
- (60) Derosa, P. A.; Seminario, J. M.; Balbuena, P. B. Properties of Small Bimetallic Ni-Cu Clusters. *J. Phys. Chem. A* **2001**, *105*, 7917.
- (61) Seminario, J. M.; Zacarias, A. G.; Castro, M. Systematic Study of the Lowest Energy States of Pd, Pd₂, and Pd₃. *Int. J. Quantum Chem.* **1997**, *61*, 515.
- (62) Seminario, J. M.; Agapito, L. A.; Yan, L.; Balbuena, P. B. Density functional theory study of adsorption of OOH on Pt-based bimetallic clusters alloyed with Cr, Co, and Ni. *Chem. Phys. Lett.* **2005**, *410*, 275.
- (63) Seminario, J. M.; Tour, J. M. Systematic Study of the Lowest Energy States of Au_n (n=1–4) Using DFT. *Int. J. Quantum Chem.* **1997**, *65*, 749.
- (64) Seminario, J. M.; Concha, M. C.; Politzer, P. A Density Functional/Molecular Dynamics of the Structure of Liquid Nitromethane. *J. Chem. Phys.* **1995**, *102*, 8281.
- (65) Habibollahzadeh, D.; Grodzicki, M.; Seminario, J. M.; Politzer, P. Computational Study of the Concerted Gas-Phase Triple Dissociations of 1,3,5-Triazacyclohexane and its 1,3,5-Trinitro Derivative (RDX). *J. Phys. Chem.* **1991**, *95*, 7699.
- (66) Politzer, P.; Seminario, J. M. Computational study of the structure of dinitraminic acid, HN(NO₂)₂ and the energetics of some possible decomposition steps. *Chem. Phys. Lett.* **1993**, *216*, 348.
- (67) Politzer, P.; Seminario, J. M. Energy Changes Associated with Some Decomposition Steps of 1,3,3-Trinitroazetidine - a Nonlocal Density-Functional Study. *Chem. Phys. Lett.* **1993**, *207*, 27.
- (68) Politzer, P.; Seminario, J.; Bolduc, P. A Proposed Interpretation of the Destabilizing Effect of Hydroxyl-Groups on Nitroaromatic Molecules. *Chem. Phys. Lett.* **1989**, *158*, 463.

- (69) Seminario, J. M.; Concha, M. C.; Politzer, P. Calculated Structures and Relative Stabilities of Euroxan, some 1,2 Dinitrosoethylenes and other Isomers. *J. Comput. Chem.* **1992**, *13*, 177.
- (70) Murray, J.; Redfern, P.; Seminario, J.; Politzer, P. Anomalous Energy Effects in some Aliphatic and Alicyclic Aza Systems and their Nitro-Derivatives. *J. Phys. Chem.* **1990**, *94*, 2320.
- (71) Derosa, P. A.; Guda, S.; Seminario, J. M. A programmable molecular diode driven by charge-induced conformational changes. *J. Am. Chem. Soc.* **2003**, *125*, 14240.
- (72) Seminario, J. M.; De La Cruz, C.; Derosa, P. A.; Yan, L. Nanometer-Size Conducting and Insulating Molecular Devices. *J. Phys. Chem. B* **2004**, *108*, 17879.
- (73) Seminario, J. M.; Araujo, R. A.; Yan, L. Negative Differential Resistance in Metallic and Semiconducting Clusters. *J. Phys. Chem. B* **2004**, *108*, 6915.
- (74) Murray, J. S.; Seminario, J. M.; Politzer, P. Does Antiaromaticity Imply Net Destabilization. *Int. J. Quantum Chem.* **1994**, *49*, 575.
- (75) Roetti, C. The CRYSTAL Code. In *Quantum-Mechanical Ab-initio Calculation of the properties of Crystalline Materials*; Pisani, C., Ed.; Springer-Verlag: Berlin, 1996; Vol. 67, p 125.
- (76) Dovesi, R.; Saunders, V. R.; Roetti, R.; Orlando, R.; Zicovich-Wilson, C. M.; Pascale, F.; Civalleri, B.; Doll, K.; Harrison, N. M.; D'Arco, P.; Llunell, M. CRYSTAL06 User's Manual; University of Torino: Torino, Italy, 2006.
- (77) Derosa, P. A.; Seminario, J. M. Electron Transport through Single Molecules: Scattering Treatment using Density Functional and Green Function Theories. *J. Phys. Chem. B* **2001**, *105*, 471.
- (78) Seminario, J. M.; Yan, L. Ab initio analysis of electron currents in thioalkanes. *Int. J. Quantum Chem.* **2005**, *102*, 711.
- (79) Salazar-Salinas, K.; Jauregui, L. A.; Kubli-Garfias, C.; Seminario, J. M. Molecular biosensor based on a coordinated iron complex. *J. Chem. Phys.* **2009**, *130*, 105101.
- (80) Jauregui, L. A.; Salazar-Salinas, K.; Seminario, J. M. Transverse Electronic Transport in Double-Stranded DNA Nucleotides. *J. Phys. Chem. B* **2009**, *113*, 6230.
- (81) Seminario, J. M.; Cordova, L. E.; Derosa, P. A. An Ab Initio Approach to the Calculation of Current-Voltage Characteristics of Programmable Molecular Devices. *Proc. IEEE* **2003**, *91*, 1958.
- (82) Seminario, J. M.; Sanders, F. C. Application of Z-Dependent Perturbation-Theory to Autoionizing States of HeliumLike Atoms-Feshbach Projection Method. *Phys. Rev. A* **1990**, *42*, 2562.
- (83) Seminario, J. M.; Derosa, P. A.; Cordova, L. E.; Bozard, B. H. A Molecular Device Operating at Terahertz Frequencies. *IEEE Trans. Nanotechnol.* **2004**, *3*, 215.
- (84) Tsukamoto, T.; Ishikawa, Y.; Sengoku, Y.; Kurita, N. A combined DFT/Green's function study on electrical conductivity through DNA duplex between Au electrodes. *Chem. Phys. Lett.* **2009**, *474*, 362.
- (85) Staykov, A.; Tsuji, Y.; Yoshizawa, K. Conductance through Short DNA Molecules. *J. Phys. Chem. C* **2011**, *115*, 3481.
- (86) Kondo, H.; Kino, H.; Nara, J.; Ohno, T. Transport properties of iron-porphyrin molecule sandwiched between Au surfaces. *Appl. Surf. Sci.* **2008**, *254*, 7985.
- (87) El-Hendawy, M. M.; El-Nahas, A. M.; Awad, M. K. The effect of constitutional and conformational isomerization on the electrical properties of diblock molecular diode. *Org. Electron.* **2011**, *12*, 1080.
- (88) James, M.; Tedesco, T.; Cassidy, D. J.; Withers, R. L. Oxygen vacancy ordering in strontium doped rare earth cobaltate perovskites $\text{Ln}_{1-x}\text{Sr}_x\text{CoO}_3\text{-}[\delta]$ ($\text{Ln} = \text{La, Pr and Nd}$; $x > 0.60$). *Mater. Res. Bull.* **2005**, *40*, 990.
- (89) Allen, F. H.; Kennard, O.; Watson, D. G.; Brammer, L.; Orpen, A. G.; Taylor, R. Tables of bond lengths determined by X-ray and neutron diffraction. Part 1. Bond lengths in organic compounds. *J. Chem. Soc., Perkins Trans. 2* **1987**, S1.